Desalination and Water Treatment
www.deswater.com

doi: 10.5004/dwt.2020.25218

183 (2020) 355–365
April

Photocatalytic remediation of treated palm oil mill effluent contaminated with phenolic compounds using TiO_2 nanomaterial

Rab Nawaz[a,*], Chong Fai Kait[a], Ho Yeek Chia[b], Mohamed Hasnain Isa[c], Lim Wen Huei[d]

[a]*Fundamental and Applied Sciences Department, Universiti Teknologi PETRONAS, 32610 Seri Iskandar, Perak, Malaysia, Tel. +60143056299; emails: rab_17000005@utp.edu.my/sankhan426@gmail.com (R. Nawaz), Tel. +60182104182; emails: chongfaikait@utp.edu.my/chongfk10@gmail.com (C.F. Kait)*
[b]*Civil and Environmental Engineering Department, Universiti Teknologi PETRONAS, 32610 Seri Iskandar, Perak, Malaysia, Tel. +60124560388; email: yeekchia.ho@utp.edu.my (H.Y. Chia)*
[c]*Civil Engineering Programme, Faculty of Engineering, Universiti Teknologi Brunei, Tungku Highway, Gadong BE1410, Brunei Darussalam, email: hasnain_isa@yahoo.co.uk (M.H. Isa)*
[d]*Advanced Oleochemical Technology Division, Palm Oil Research Institute of Malaysia, 43000 Bandar Baru Bangi, Kajang, Selangor, Malaysia, Tel. +60126901371; email: limwen@mpob.gov.my (L.W. Huei)*

Received 19 May 2019; Accepted 20 November 2019

ABSTRACT

The photocatalytic remediation efficiency of treated palm oil mill effluent (POME) containing phenolic compounds was investigated employing TiO_2 nanomaterial. The TiO_2 was produced via chemical precipitation method using $TiCl_4$ as a precursor, water and aqueous glycerol solution as synthesis media. The structural, optical, morphological and textural properties of TiO_2 were analyzed by Raman spectroscopy and X-ray diffraction, diffuse reflectance UV-Visible spectroscopy, field-emission scanning electron microscopy and Brunauer–Emmet–Teller total surface area analysis. The results demonstrated that TiO_2 synthesized in aqueous glycerol solution exhibited an excellent redshift of the optical response into the visible light region with a narrow bandgap of 2.96 eV which led to improved remediation efficiency of treated POME. The particle size range of TiO_2 prepared with and without glycerol was 14.98–24.51 nm and 13.02–17.37 nm, respectively. The effect of TiO_2 loading and H_2O_2 dosage were optimized using a central composite design and their optimum levels were determined as 0.9 g/L and 1.5985 mol/L, respectively. Under the optimized conditions, 78.32% of 224.85 mg/L phenolic compounds were degraded within 180 min of visible light irradiation using the glycerol-mediated synthesized TiO_2. For comparison, the performance of TiO_2 photocatalyst prepared in water achieved 67% photocatalytic degradation of phenolic compounds in treated POME.

Keywords: TiO_2 synthesis; Glycerol; Optical absorption; Treated POME; Phenolic compounds; Photocatalytic remediation

1. Introduction

Phenolic compounds are present in many industrial effluents due to their widespread use in several manufacturing processes. Palm oil mill effluent (POME), for instance, has been reported to contain more than 1,000 mg/L of phenols [1,2]. Conventional methods viz, anaerobic digestion and anaerobic ponding system, commonly adopted in Southeast Asia for POME treatment, are ineffective in degrading phenolic compounds due to their toxicity on microorganisms. High levels of phenols ranging from 33 to 630 mg/L have been reported previously in treated POME [3,4]. High toxicity, bioaccumulation potential, negative human health and environmental impacts of phenolic compounds and

* Corresponding author.

stringent regulatory standards necessitate the search for an effective treatment method to remove phenolic compounds from treated POME before its final release into the ecosystem [2,5,6].

Various physicochemical and biological treatment methods have been explored for the removal of phenolic compounds from industrial effluents [7–10]. Biological treatment using different types of microorganisms has been widely investigated for the elimination of phenolic compounds from waste effluents originating from agro-industries, especially the oil palm industry [4,11,12]. The results from these investigations were encouraging. For example, *Trametes hirsute* strain AK 0_4 used in anaerobic digestion effectively removed phenols up to 82.2% of 112 mg/L after 8 d of retention time [11]. However, biological treatment has several major limitations: firstly, they are not effective for complete removal of phenolic compounds to comply with standard discharge limit; secondly, enormous amount of nutrients are required by microorganisms coupled with difficulty in obtaining their special strains; thirdly, they require long retention time and last but not least, it produces secondary pollutant in the form of sludge [13].

Photocatalytic treatment using TiO_2 nanomaterial has the potential to replace or augment the existing treatment methods for the remediation of treated POME. Despite the high efficiency and other associated benefits such as predominant photocatalytic activity, low toxicity, high resistance towards corrosion, low production cost of TiO_2, complete mineralization, rapid reaction rates and operation under ambient conditions of pressure and temperature [14–17], scientific literature is scarce regarding the use of photocatalytic treatment for the remediation POME [18]. Only a few research groups have investigated photocatalytic remediation of POME. For instance, 26.77% photocatalytic degradation of POME with initial chemical oxygen demand (COD) ranging from 155 to 170 ppm by silver doped titanium dioxide under visible light was achieved [19]. Similarly, another group investigated the photo-mineralization of POME over TiO_2 under UV irradiation [20]. Their results showed that, in the presence of O_2, the COD degradation of POME reached 78.0% after 20 h of UV irradiation. However, there seems to be no work reported in the literature regarding the photocatalytic treatment of phenolics-laden treated POME.

The efficiency of a photocatalytic system can be enhanced by optimizing the process variables, such as photocatalyst loading, oxidant dosage, pollutant concentration, pH, light intensity and flow rate. Conventionally, optimization has been carried out using changing one factor at a time (OFAT) approach. This is an inefficient way for optimization of process variables because (i) OFAT approach does not allow to study the combined and interaction effects of two or more independent variables, and (ii) The approach is also laborious and time-consuming [21,22]. Thus, response surface methodology (RSM), which is a statistical method that includes the effects of individual factors as well as their interactions on the outcome variables, has become a choice in many studies [23–27]. The approach has made the optimization process easier.

In the present work, the TiO_2 nanomaterial was prepared via precipitation method using water and aqueous glycerol solution as synthesis media and $TiCl_4$ as the precursor. The effect of glycerol on crystalline structure, optical absorption property and bandgap, textural properties, and surface morphology of TiO_2 was investigated. The synthesized TiO_2 was employed for photocatalytic remediation of treated POME containing phenolic compounds. Also, the effects of operational variables viz, TiO_2 loading and hydrogen peroxide (H_2O_2) dosage were investigated and optimized employing central composite design (CCD) based on RSM.

2. Experimental

2.1. Chemicals

Titanium tetrachloride ($TiCl_4$, 99.9%), glycerol (85%), ammonium hydroxide (NH_4OH, 30%), Folin–Ciocalteu phenol reagent (99%), sodium carbonate (Na_2CO_3, 99.9%), ethyl acetate and Gallic acid (99%) were purchased from Merck, Malaysia. All the chemicals were used without further purification.

2.2. Synthesis of TiO_2 nanoparticles

TiO_2 nanoparticles were synthesized via precipitation method. $TiCl_4$ was used as a Ti precursor where 0.10 moles were transferred dropwise into 50 mL of 1.163 M aqueous glycerol solution and cooled in an ice bath. Vigorous stirring was maintained throughout the reaction. TiO_2 precipitates were obtained by adding NH_4OH (2.5 M) into the mixture until pH 10 followed by centrifugation at 6,000 rpm for 10 min. The TiO_2 precipitates were rinsed several times with deionized water to remove impurities and dried for 24 h in an oven at 80°C. The dried powder was crushed, grounded and transferred to a porcelain boat for calcination at 300°C for an h in a muffle furnace. For ease in referencing, the TiO_2 prepared with glycerol was labeled as TG300. The TiO_2 nanoparticles were also synthesized in water without the presence of glycerol following the procedure describe for TG300, as a reference for comparison purpose. The TiO_2 prepared without the presence of glycerol were denoted as T300.

2.3. Material characterization

Raman spectra were obtained using (Inspector 500) spectrometer at an excitation wavelength of 532 nm with a solid-state diode laser having a power of 25 mW. The material was characterized using X-ray diffraction (XRD) (PANalytical X'Pert3 Powder, AA Almelo, The Netherlands). Both techniques were employed to determine the type of phases present on the particles. The diffuse reflectance UV-Visible spectroscopy (DRUV-Vis) absorption spectra were recorded using an Agilent Cary 100 spectrophotometer (Santa Clara, CA, USA) where Spectralon was used as the reference. Data from DRUV-Vis were also represented in the form of Tauc's plot which was employed for bandgap determination. The particle size range and surface morphology were obtained from field-emission scanning electron microscopy (FESEM) images captured by the Carl Zeiss instrument, Oberkochen, Germany (SUPRA 55VP). Energy-dispersive X-ray spectroscopy (EDX) spectrum and mapping were accomplished with the same instrument. The Brunauer–Emmet–Teller (BET) specific surface area, pore size and pore volume of the TiO_2 samples were measured from N_2 adsorption–desorption

isotherms acquired with (Micromeritics Corps., Norcross, GA, USA) instrument.

2.4. Analytical method

Treated POME sample was collected from the final pond of the wastewater treatment plant of a local palm oil mill situated in the state of Perak, Malaysia. Prior to analysis, the treated POME sample was centrifuged at 7,000 rpm (Heraeus Biofuge primo, William Scientific, Dassel, Germany) for 10 min to remove the residual solids. The total phenolic content of the treated POME was determined spectrophotometrically with a slight modification of the Folin–Ciocalteu (F–C) analytical technique as described by Ergul et al. [28]. According to this method, 0.1 mL of 5-fold diluted treated POME sample was mixed with 0.5 mL of four-fold diluted F–C phenol reagent. After 5 min of retention time, the sample was kept for an h at ambient temperature after the addition of 0.5 mL of Na_2CO_3 (200 g/L). Finally, the absorbance measurement was recorded at 765 nm with the help of a spectrophotometer, SpectroVis Plus® instrument (SW Millikan Way Beaverton, OR 97005, USA) and compared with the calibration curve of gallic acid standards.

2.5. Visible light photocatalytic evaluation

The photocatalytic activity of TG300 and T300 was assessed by monitoring the degradation of total phenolic compounds from treated POME under visible light illumination. The experimental setup for carrying out photocatalytic experiments is shown in Fig. 1. The photocatalytic reactions were performed in a batch mode in a 250 mL Pyrex photoreactor with a quartz window (Internal diameter, 7.0 cm and height, 9.0 cm) tightly sealed at the top. Preliminary photocatalytic reactions were performed to determine the suitability of the synthesized TiO_2 materials (TG300 and T300) for the degradation of phenolic compounds. An accurately weighed TiO_2 NPs (0.5 g/L) were dispersed in 50 mL of treated POME (initial concentration of phenolic compounds was 224.85 mg/L). The suspension was vigorously stirred for 30 min in the dark for achieving equilibrium prior to irradiation with a halogen lamp at 3.9 W/cm^2 light intensity which was fixed 10 cm above the photoreactor. The strong heating and evaporation effect was negligible since the temperature of the photoreactor was maintained by using an electric cooling fan. The photoreactor was tightly sealed to prevent evaporation of the working solution. An aliquot of 1 mL was taken from the photoreactor at 60 min interval for 180 min duration. The solid particles were removed from the samples prior to analysis of phenolic compounds concentration. The degradation efficiency was monitored by examining the concentration of phenolic compounds by using Eq. (1) as given below:

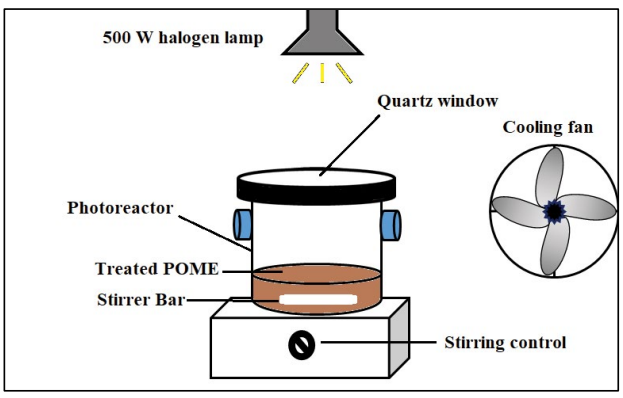

Fig. 1. Experimental setup of photocatalytic reactions.

$$X\% = \frac{C_i - C_f}{C_i} \times 100\% \quad (1)$$

where X% is the degradation efficiency of phenolic compounds after 180 min of reaction, C_i is the initial concentration and C_f is the final concentration of phenolic compounds.

Another set of photocatalytic reactions under continuous stirring and visible light irradiation for 180 min was conducted for detailed investigation and optimization of the process factors viz, TiO_2 loading and H_2O_2 dosage. Photocatalytic experiments were carried out at different TiO_2 loading (0.4, 0.9, 1.4 g/L) and H_2O_2 dosage (0.8445, 1.5985 and 2.2759 mol/L). An aliquot of 10 mL were withdrawn from the photoreactor at the end of the reaction (180 min) and analyzed for phenolic compounds concentration. The photocatalytic degradation efficiency was calculated using Eq. (1).

2.6. Experimental design

RSM based on CCD, composing of a factorial model was used as a tool for designing photocatalytic reactions and optimization of the process variables. The CCD was composed of three-levels of variables, three replicated central points and star points. TiO_2 loading (A) and H_2O_2 dosage (B) were chosen as quantitative while the type of TiO_2 (C) was designated as qualitative independent variables. The percentage of degradation of phenolic compounds was chosen as the response factor.

The real values and coded levels of the independent factors are presented in Table 1. TiO_2 loading and H_2O_2 dosage were varied over a range of 0.4 to 1.4 g/L and 0.8445 to 2.2759 mol/L, respectively. The range over which the variables were varied was identified previously as being sufficient to actually show a difference in the degradation, but not so large as to move the system to a totally different operational regime [29]. The optimization procedure consisted of changing the variable levels to identify the most favorable conditions for the photocatalytic degradation of phenolic compounds by carrying out a total of 22 experiments.

The data were analyzed using statistical software (Design Expert v.10.0.0; Stat-Eas Inc., USA) to get the associated polynomial for the photocatalytic system and to build the response surface plots. The mathematical model was statistically validated using analysis of variance test (ANOVA) with the same software and by comparison of the experimental values with predicted values by the model.

3. Results and discussion

3.1. Structural and optical characteristics

Raman scattering was measured to examine the crystalline structure of TiO_2 NPs synthesized with glycerol (TG300)

and without glycerol (T300). The Raman spectra of both the samples are shown in Fig. 2a. Raman active modes with frequencies at 167, 399, 515, and 640 cm^{-1} were observed for TG300 and T300. These modes are conforming to the characteristic anatase phase of TiO_2 [30]. No weakening or broadening of the scattering peaks nor additional vibrational modes of rutile or brookite were observed for TG300, corroborating that the crystal structure is not affected by the presence of glycerol. The Raman results were consistent with XRD patterns as given in Fig. 2b, where the diffraction peaks observed at 2θ = 25.3°, 37.9°, 47.9°, 54.3°, 63.0°, 69.7°, and 75.4° assigned to (101), (004), (105), (211), (204), (116), and (220) planes, respectively for anatase TiO_2. The results of XRD are consistent with the previous report [31]. The presence of the main and sharp diffraction peak of the anatase crystalline phase at 2θ = 25.3° is consistent with the Raman scattering results. Sharp peaks are observed around 167 cm^{-1} in Raman spectra and XRD diffractogram (2θ = 25.3°) indicating the high crystallinity of TG300 and T300. High crystallinity is desirable because it can minimize electron-hole pair recombination during photoreactions [32].

Table 1
Real and coded levels of independent process factors

Factors	Levels		
	–1	0	+1
TiO_2 loading g/L (*A*)	0.4	0.9	1.4
H_2O_2 dosage mol/L (*B*)	0.8445	1.5985	2.2759
Type of TiO_2 (*C*)	T300		TG300

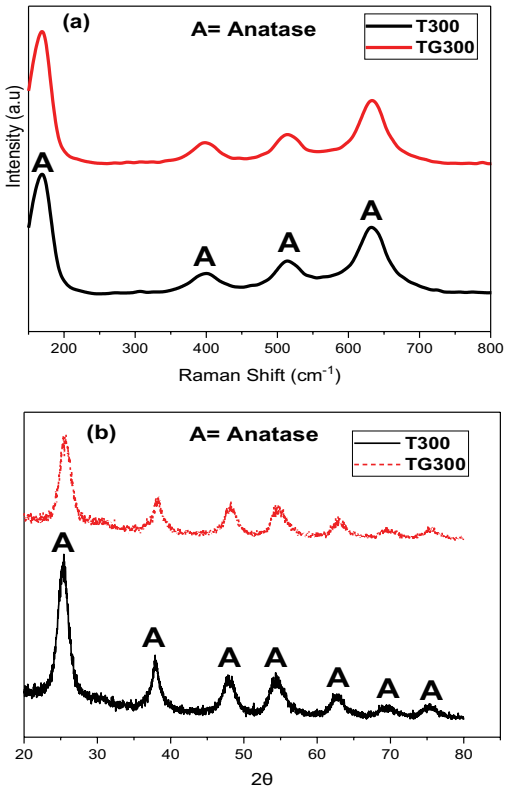

Fig. 2. Raman spectra (a) and XRD diffractogram (b) of the TiO_2 prepared with and without glycerol.

The DRUV-Vis spectra for both types of TiO_2 NPs, TG300 and T300 are shown in Fig. 3a. The spectra clearly show broad absorption edges, beginning from 400 nm and extending into the visible spectral region. The intensity of light absorption increased with the incorporation of glycerol, which is consistent with the color change from off-white (T300) to black (TG300) after calcination at 300°C as shown in Fig. 3a (inset). The color of the material is previously correlated with the absorption of light. It is reported that if a material absorbs only a certain percentage across the whole visible-light region equally, it is partially black or grey [33]. As shown in Fig. 3a, the absorption spectrum for T300 showed a typical absorbance edge at 400 nm while the absorption edge was extended beyond 400 nm for TG300. The optical absorption results demonstrated that the use of glycerol as co-solvent for the synthesis of TiO_2 can significantly improve the visible light harvesting property ranging from 400–800 nm. The bandgap energies for TG300 and T300 were determined by plotting the Tauc's plot $(F(R)\cdot hv)^{1/2}$ verses hv plot and extrapolating the linear part of the graph to the x-axis at $\alpha = 0$ as shown in Fig. 3b. The bandgap for TG300 and T300 was 2.96 and 3.17 eV, respectively indicating

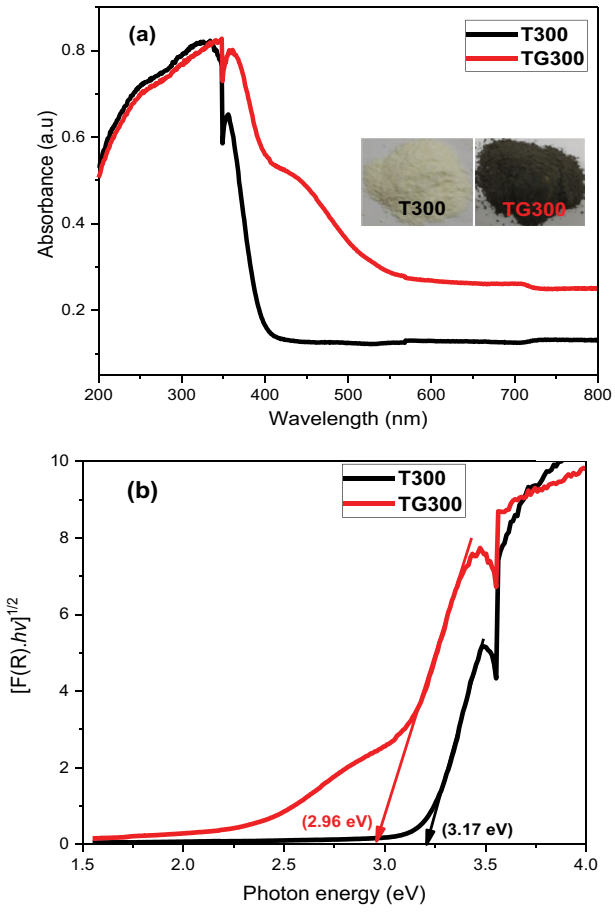

Fig. 3. (a) DRUV-Vis spectra and images (inset) and (b) Tauc's plot $(F(R)\cdot hv)^{1/2}$ vs. hv plot of the TiO_2 prepared with and without glycerol.

that the presence of glycerol during TiO_2 synthesis can significantly reduce the bandgap. The bandgap of TG300 was reduced significantly compared to pure anatase phase TiO_2 as reported by Gonzalez-Reyes et al. [34]. As a result, the electron in black TiO_2, TG300 can be more easily excited from the valence band with better charge separation achieved by efficient visible light absorption [35]. It is well documented that TiO_2 having a narrow bandgap may be appropriate for photocatalytic applications especially in wastewater remediation [36].

3.2. Morphology, particle size, and specific surface area

The morphology of both TG300 and T300 was observed from FESEM images given in Figs. 4a and b. In Fig. 4a, T300 showed spherical shaped particles. The spherical shape was maintained in TG300 prepared with the presence of glycerol and the particles were more agglomerated (Fig. 4b). The particle sizes of both the samples were estimated from FESEM images. Table 2, lists the particle size range of TiO_2 prepared with and without glycerol. The TG300 showed a rather larger average particle size range (14.98–24.51 nm) as compared to T300 (13.02–17.37 nm). The larger particles formation in the presence of glycerol can be attributed to the synthesis route followed for the synthesis of TiO_2 [37], rather than the presence of glycerol. Previously, it has been reported that using glycerol as co-solvent can promote smaller particle formation [38]. Their results substantiated that glycerol may play a very essential role as a templating agent and the presence of glycerol as co-solvent make the solution highly viscous. For these reasons the diffusion of the TiO_2 nuclei to form larger particles and the

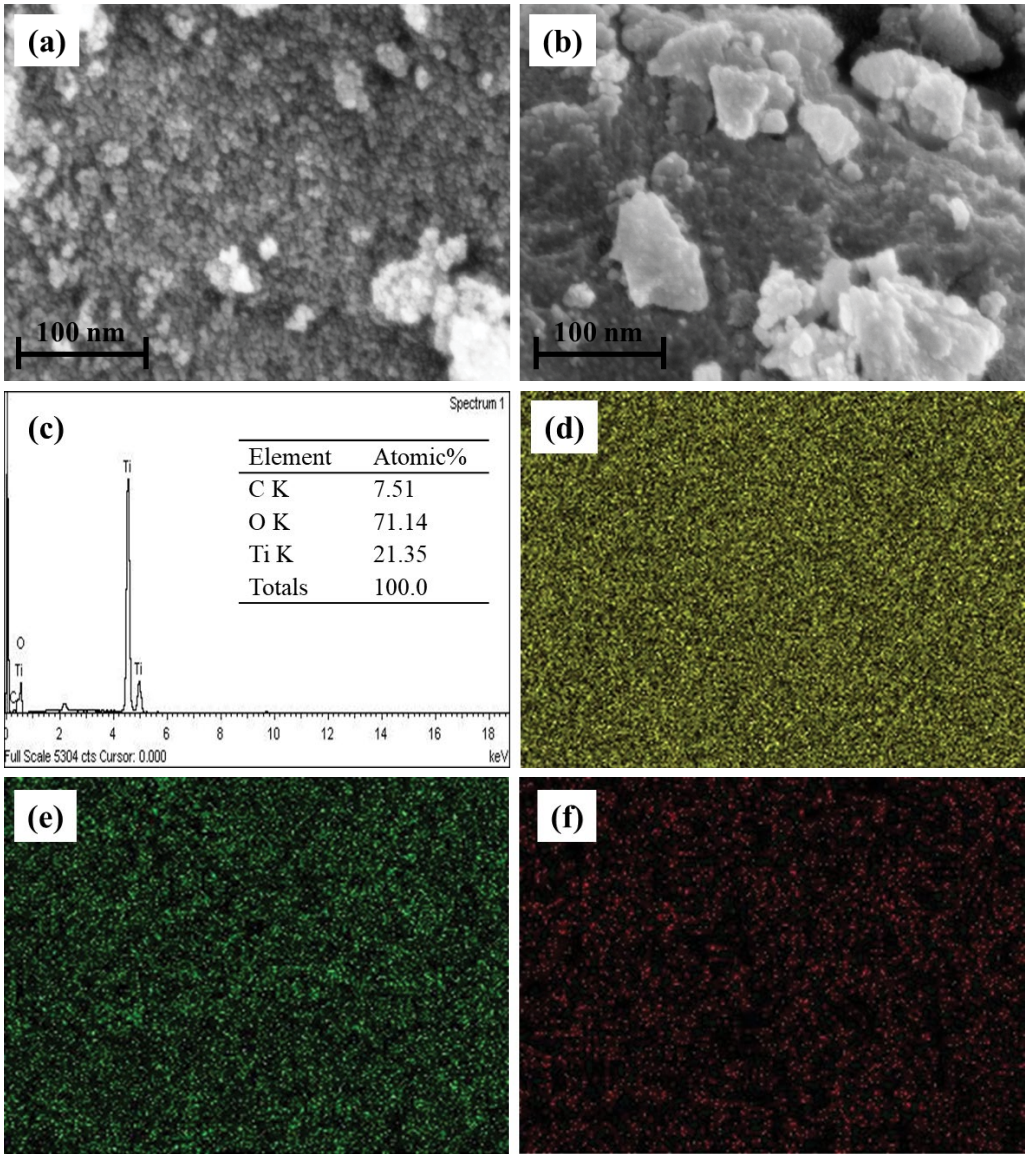

Fig. 4. FESEM images of TiO_2 NPs (a) T300, (b) TG300, (c) EDX spectrum of TG300, and EDX mapping for (d) titanium, (e) oxygen, and (f) carbon.

Table 2
Properties of TiO_2 prepared with and without glycerol

Sample	Bandgap (eV)	FESEM particle size range (nm)	BET specific surface area (m^2/g)	Pore volume (cm^3/g)	Pore size (nm)
T300	3.17	13.02–17.37	154.51	0.207	3.872
TG300	2.96	14.98–24.51	99.88	0.166	4.799

agglomeration of the nanoparticles could be difficult or remarkably decreased. The EDX spectrum and mapping of TG300 as a reference are presented in Figs. 4c and d, respectively. The mapping and spectrum both showed the carbon content is an extra component of TG300 which can be due to instrumental impurities.

The textural properties viz, specific surface area, pore volume and pore size distribution of TG300 and T300 are presented in Table 2 and Fig. 5. Both types of TiO_2 showed typical behavior of mesoporous material, with low energy of adsorption as was inferred from the N_2 adsorption-desorption isotherms shown in Fig. 5a. According to International Union of Pure and Applied Chemistry classification, the N_2 adsorption–desorption isotherms of the synthesized TiO_2 NPs exhibited type IV isotherms and H2-type hysteresis loop. This type of isotherm occurs on the surface of mesoporous material where monolayer formation is followed by capillary condensation and the forward process (adsorption) is not equal to a backward process (desorption). The desorption branch is steeper than the adsorption branch in the hysteresis loop. This is due to the blocking of pores by larger pore bodies emptying into smaller pore neck. The TiO_2 prepared in the presence of glycerol has shown a complex pore network with ill-defined structure and wider pore size distribution compared to TiO_2 prepared in the absence of glycerol showing regular mesoporous channels. Due to the increased mesopore size, the TG300 has shown less adsorption with a shift in the hysteresis loop at a high relative pressure (P/P_0 = 1) [39]. On the other hand, T300 exhibited more surface area of 154.51 m^2/g and a relatively larger pore volume of 0.207 cm^3/g. After the inclusion of glycerol, the BET specific surface area reduced by about 35% to 99.88 m^2/g with a relatively smaller pore volume (0.166 cm^3/g). This result indicates the partial blocking of the pore by glycerol. The smaller surface area of the TiO_2 synthesized in the presence of glycerol was correlated with its larger particle size estimated from FESEM images. The larger the particle size, the lower the surface area. It is worth noted here that both types of TiO_2 NPs showed a larger surface area when compared to the previously reported commercial TiO_2 photocatalyst (Degussa P25, Frankfurt, Germany). The specific surface area of the TG300 and T300 was about 50% and 34% more than previously reported sol–gel titania (74 m^2/g) by Garcia-Montelongo et al. [40]. The surface area of T300 was 67% while that of TG300 was 49% more than the previously reported commercial titania (50 m^2/g) [41]. The pore size distribution curve of TG300 and T300 is presented in Fig. 5b. The TiO_2 prepared in the presence of glycerol showed a larger pore size indicated by the sharp peak observed at 4.799 nm in the pore size distribution curve. The TiO_2 prepared without glycerol showed a comparatively smaller pore size (3.872 nm). The results of pore size distribution are consistent with the N_2 adsorption-desorption isotherms and the pore size was correlated with surface area, the larger the pore size the smaller the surface area.

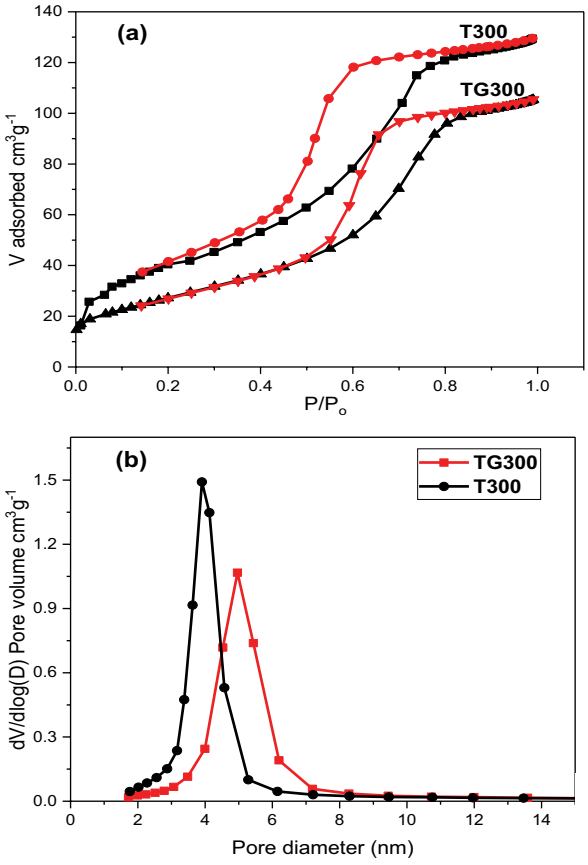

Fig. 5. (a) N_2 adsorption–desorption isotherms and (b) pore size distribution of the TiO_2 prepared with and without glycerol.

3.3. Preliminary photocatalytic results

Preliminary photocatalytic experiments were carried out to determine the ability of the TiO_2 NPs synthesized with and without glycerol to act as a photocatalyst for the degradation of phenolic compounds from treated POME matrix. The degradation profile of phenolic compounds in treated POME matrix under non-optimized conditions is presented in Fig. 6. Experiments carried out in the dark showed that the adsorption of phenolics on the photocatalyst surface is insignificant at normal initial pH (7.6) of treated POME solution. Conversely, when the solution was irradiated with

visible light without any photocatalyst, minor photolysis was observed. A notable enhancement in phenolic compounds degradation was witnessed when 0.5 g/L TiO_2 was suspended into the treated POME solution, indicating the appropriate photoactivity of the material. The photocatalytic degradation of phenolic compounds reached 25% and 32% for 180 min of irradiation at photocatalyst loading of 0.5 g/L for TG300 and T300, respectively. These results confirm the photocatalytic activity of the prepared photocatalysts, which were then further used for optimization study.

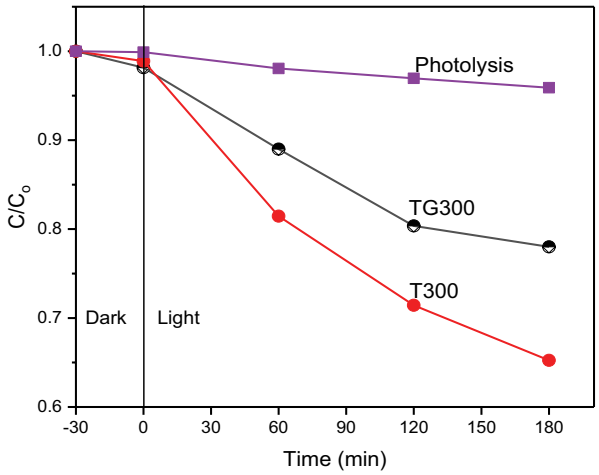

Fig. 6. Degradation profile of phenolic compounds under non-optimized conditions by TiO_2 photocatalysis after 180 min visible light irradiation at 0.5 g/L photocatalyst loading.

3.4. Statistical analysis

The data obtained from photocatalytic experiments carried out under various operating conditions was analyzed statistically. The photocatalytic degradation of phenolic compounds was measured as an outcome. Experimental design (CCD), the experimental and predicted percentage photocatalytic degradation of phenolic compounds are presented in Table 3. A polynomial equation consisting of eight coefficients was obtained from the design expert software. The empirical model showing the relationship between photocatalytic degradation of phenolic compounds and independent variables is presented as Eq. (2):

$$Y = 75.19 + 2.06A + 1.78B - 2.90C - 6.30AB - 0.046AC - 0.65BC - 9.28A^2 - 7.79B^2 \quad (2)$$

where Y represents the degradation efficiency, A and B denote the coded values of TiO_2 loading and H_2O_2 dosage, respectively and C represents the type of TiO_2. A positive sign in front of the model terms in the polynomial showed a beneficial individual or combined effect of TiO_2 loading and

Table 3
Experimental results from CCD of photocatalytic degradation of phenolics from treated POME

Run	(A): TiO_2 loading (g/L)	(B): H_2O_2 dosage (mol/L)	(C): Type of TiO_2	Degradation (%)	
				Experimental	Predicted
1	1.4	2.2759	TG300	59.31	59.27
2	1.4	2.2759	T300	51.57	52.08
3	0.4	2.2759	TG300	68.62	67.64
4	0.4	1.5985	TG300	66.01	66.40
5	0.4	0.8445	TG300	50.23	50.19
6	1.4	0.8445	TG300	66.56	67.00
7	0.9	0.8445	T300	62.89	63.37
8	1.4	1.5985	TG300	71.65	70.92
9	0.9	2.2759	TG300	71.26	72.73
10	1.4	0.8445	T300	62.29	62.40
11	0.9	1.5985	TG300	78.23	78.03
12	0.9	2.2759	T300	66.41	65.63
13	0.9	1.5985	T300	73.14	72.28
14	0.9	1.5985	TG300	77.93	78.09
15	0.9	0.8445	TG300	67.83	67.87
16	0.4	2.2759	T300	60.84	60.63
17	0.9	1.5985	TG300	77.01	78.16
18	0.9	1.5985	T300	72.39	72.28
19	0.4	1.5985	T300	59.42	60.99
20	1.4	1.5985	T300	65.34	65.02
21	0.4	0.8445	T300	46.83	45.77
22	0.9	1.5985	T300	71.68	72.39

H_2O_2 dosage. A negative sign denotes the antagonistic effect of these two independent variables on the photocatalytic degradation of phenolic compounds in treated POME [42].

The empirical model was validated by performing ANOVA for the regression test. The significance of each factor was identified through Fisher's values (*F*-value) and probability values (*P*-value). *P* values lower than 0.05 and higher *F* values show the statistical significance of factors affecting experimental outcomes [43,44]. Fisher's values and probability values for all the model terms are listed in Table 4. The high *F*-value (234.05) showed the significance of the mathematical model. The chance that such high value could arise due to noise is only 0.01%. *P*-values lower than 0.05 indicated the significance of the model terms. In the current case TiO_2 loading, H_2O_2 dosage, type of TiO_2, interaction between TiO_2 loading, the interaction of TiO_2 loading and type of TiO_2 and higher levels of TiO_2 loading and H_2O_2 dosage are significant model terms that affect photocatalytic degradation of phenolic compounds in treated POME matrix. The results exposed that the photocatalytic degradation of phenolic compounds was enhanced by TiO_2 loading (*A*) and H_2O_2 dosage (*B*) with *P*-values of 0.0001 and 0.0001, respectively. The F-statistic, confirmed the model fitting to the experimental data as the *P*-value was more than 0.05 indicating the insignificance of the lack of model fitting. Since we want the model to fit, the insignificant lack of fit is good.

The model fit was further verified from the determination coefficient value (R^2). The R^2 value refers to the proportion of change in the outcome accounted for the experimental independent variables and their interactive effects [45]. In this study, the R^2 value of 0.9932 suggests that 99.3% of the observed variation in the outcome can be due to the variation or change in the model terms. The predicted R^2 value of 0.977 is in reasonable agreement with adjusted R^2 (0.988) showing the difference of less than 0.2. This confirmed a reasonable adjustment of the model to experimental results. The mathematical model was also validated by comparing predicted and experimental results as shown in Fig. 7.

3.5. Optimization of the process variables

An experimental design was created to identify the optimum operating conditions for the factors affecting the photocatalytic process. The two most influential factors viz, TiO_2 loading and H_2O_2 dosage were considered. The variables were simultaneously changed to identify the conditions most favorable for the degradation of phenolic compounds in treated POME. A 3D illustration of the polynomial is presented in Fig. 8 where it can be observed that the percentage of degradation is enhanced with increasing TiO_2 loading and H_2O_2 dosage. Based on the results, the optimized reaction conditions were reached using a polynomial equation; optimum levels for TiO_2 loading and H_2O_2 dosage are found at 0.9 g/L and 1.5985 mol/L, respectively. Further experiments were performed under the optimized conditions, obtaining 78.32% and 67.0% of total phenolic compounds degradation under 180 min of visible light radiation, showing a considerable enhancement as compared to preliminary studies where only 25% and 32% degradation was achieved in 180 min, using TG300 and T300, respectively. The use of H_2O_2 as an oxidant in combination with TiO_2 enhanced the photocatalytic degradation of phenolic compounds which is consistent with previous studies [46,47]. The improvement in photocatalytic degradation can be attributed to additional hydroxyl radicals produced by H_2O_2, which are vital for reacting with the pollutant and preventing the recombination of photogenerated electron-hole pair [48]. Under the optimized conditions, TG300 prepared in the presence of glycerol performed better (Fig. 8a) compared to T300 prepared without glycerol (Fig. 8b). The improved photocatalytic activity of TiO_2 NPs prepared with glycerol can be attributed to its black color which facilitates the efficient visible light harvesting. The enhanced photocatalytic activity of black TiO_2 (TG300) can also be attributed to its narrow bandgap [49] and better charge separation [50]. The electron in black TiO_2 can be more easily ejected from the valence band by irradiation with visible light resulting in electron-hole pair generation. It is well documented that the photoactivity of TiO_2 not only rely on specific surface area but also on the number of exciting charges on its surface and the number of exciting charges are dependent on the light absorption. The more light being absorbed by TiO_2, the more charge carriers are likely to be present on the surface to perform photoreactions [51,52]. By shifting the optical response of TiO_2 to the

Table 4
Regression analysis of the model terms

Term	*f*-value	*p*-value
A	234.05	<0.0001
B	59.57	<0.0001
C	44.38	<0.0001
AB	215.84	<0.0001
AC	369.51	<0.0001
BC	0.029	0.8666
A^2	5.85	0.0310
B^2	357.85	<0.0001

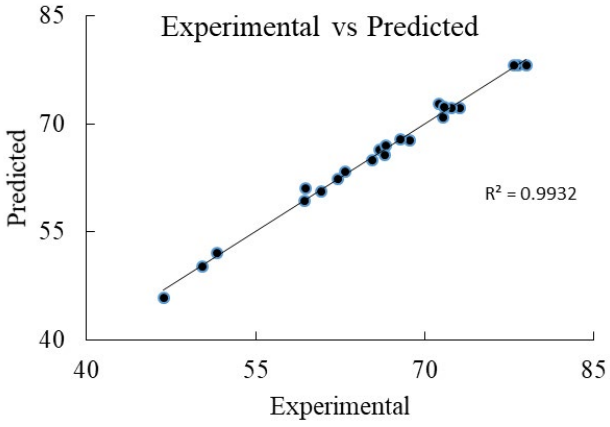

Fig. 7. Experimental results plotted vs. the results predicted by the mathematical model.

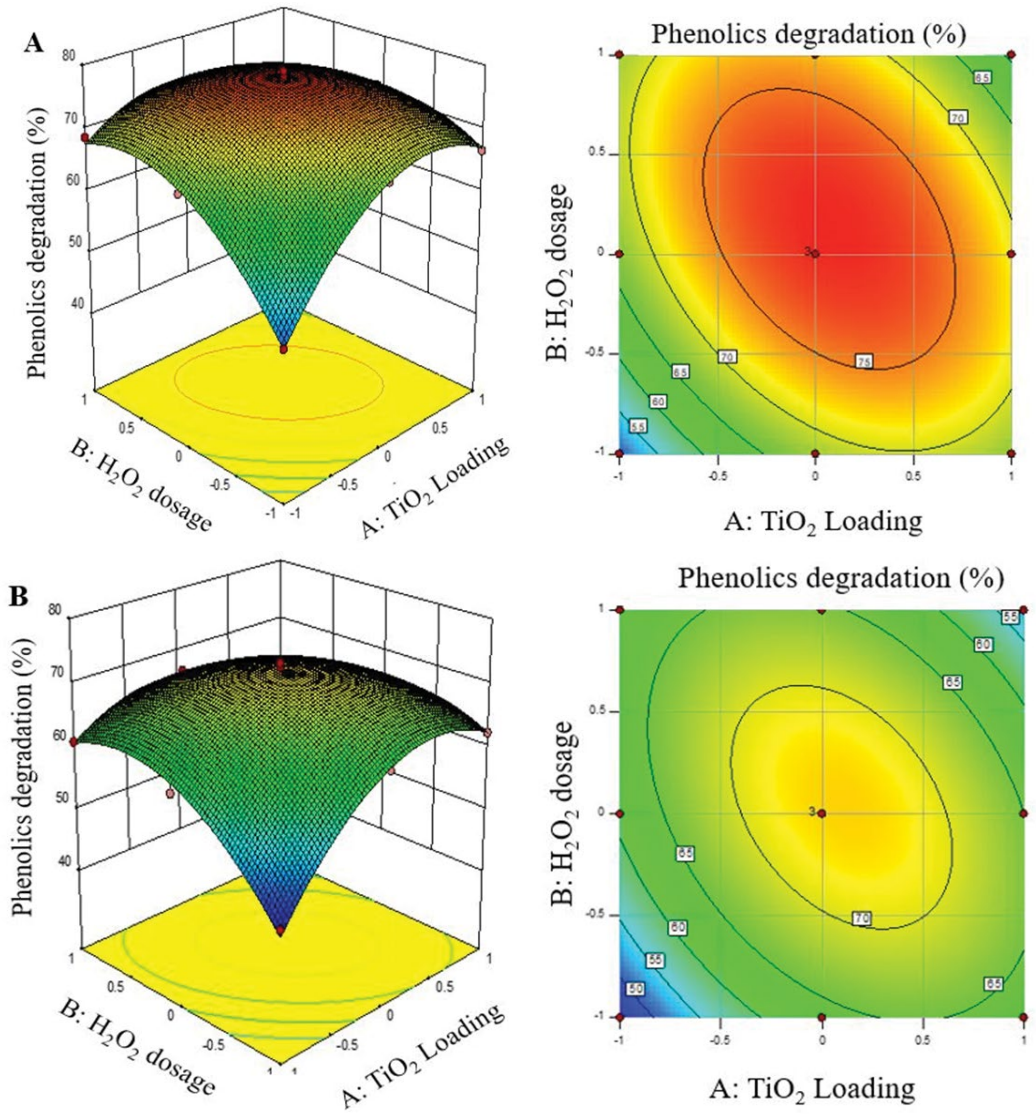

Fig. 8. Response surface (left) and contour plots (right) for phenolic compounds degradation at 180 min of visible light irradiation by the TiO_2 prepared in the presence of glycerol (a) and without glycerol (b).

visible spectral range clearly improved its overall photoactivity despite its lower surface area.

4. Conclusion

In this study, black TiO_2 nanoparticles (TG300) which exhibited anatase phase were successfully synthesized via precipitation method using $TiCl_4$ as Ti precursor and in aqueous glycerol medium. The TiO_2 NPs (TG300) prepared in the presence of glycerol have 14.98–24.51 nm average particle size range while that of T300 was 13.02–17.37 nm. The optical response of the TiO_2 was extended into the visible spectral range (λ > 400 nm) in the presence of glycerol. The TiO_2 prepared in the presence of glycerol showed a significant reduction in the bandgap (2.96 eV) compared to TiO_2 prepared in the absence of glycerol (3.17 eV). The narrow bandgap of the TiO_2 synthesized in the presence of glycerol has led to an enhanced visible-light photocatalytic activity which was confirmed by efficient photodegradation of phenolic compounds in treated POME. The mathematical model from CCD was successfully employed for the optimization of the process variables and the optimized conditions for the degradation of phenolic compounds from treated POME were achieved. Under the optimized levels of TiO_2 loading (0.9 g/L) and H_2O_2 dosage (1.5985 mol/L), 78.32% of the 224.85 mg/L phenolic compounds were degraded in 180 min under visible light illumination.

Acknowledgements

This work is supported by Yayasan Universiti Teknologi PETRONAS(YUTP-153AA-E72) Malaysia. We are grateful for the Laboratory Management Unit of UTP (LMD-UTP) which kindly provided its facilities. The first author would like to thank UTP for the award of Graduate Assistantship (GA). Authors also acknowledge support from the Fundamental

and Applied Sciences Department, Centre of Nanostructures and Nanodevices (COINN) and Centralized Analytical Laboratory (UTP) for material characterization.

References

[1] M.Z. Alam, E.S. Ameem, S.A. Muyibi, N.A. Kabbashi, The factors affecting the performance of activated carbon prepared from oil palm empty fruit bunches for adsorption of phenol, Chem. Eng. J., 155 (2009) 191–198.

[2] P. Khongkhaem, O. Suttinun, A. Intasiri, O. Pinyakong, E. Luepromchai, Degradation of phenolic compounds in palm oil mill effluent by silica-immobilized Bacteria in internal loop airlift bioreactors, CLEAN-Soil Air Water, 44 (2016) 383–392.

[3] P. Phonepaseuth, V. Rakkiatsakul, B. Kachenchart, O. Suttinun, E. Luepromchai, Phenolic compounds removal by grasses and soil bacteria after land application of treated palm oil mill effluent: a pot study, Environ. Eng. Res., 24 (2018) 127–136.

[4] P. Tosu, E. Luepromchai, O. Suttinun, Activation and immobilization of phenol-degrading bacteria on oil palm residues for enhancing phenols degradation in treated palm oil mill effluent, Environ. Eng. Res., 20 (2015) 141–148.

[5] X. Sun, C. Wang, Y. Li, W. Wang, J. Wei, Treatment of phenolic wastewater by combined UF and NF/RO processes, Desalination, 355 (2015) 68–74.

[6] F. Banat, S. Al-Asheh, L. Al-Makhadmeh, Utilization of raw and activated date pits for the removal of phenol from aqueous solutions, Chem. Eng. Technol., 27 (2004) 80–86.

[7] L.G.C. Villegas, N. Mashhadi, M. Chen, D. Mukherjee, K.E. Taylor, N. Biswas, A short review of techniques for phenol removal from wastewater, Curr. Pollut. Rep., 2 (2016) 157–167.

[8] B.K. Ghosh, N.N. Ghosh, Applications of metal nanoparticles as catalysts in cleaning dyes containing industrial effluents: a review, J. Nanosci. Nanotechnol., 18 (2018) 3735–3758.

[9] C.R. Fonseca, J.L. Paiva, E.M. Rodriguez, F.J. Beltran, A.C.S.C. Teixeira, Degradation of phenolic compounds in aqueous sucrose solutions by ozonation, Ozone Sci. Eng., 39 (2017) 255–263.

[10] L. Zhou, H. Cao, C. Descorme, Y. Xie, Phenolic compounds removal by wet air oxidation based processes, Front. Environ. Sci. Eng., 12 (2018) 1–20.

[11] A. Kietkwanboot, H.T.M. Tran, O. Suttinun, Simultaneous dephenolization and decolorization of treated palm oil mill effluent by oil palm fiber-immobilized *Trametes Hirsuta* strain AK 0_4, Water Air Soil Pollut., 226 (2015) 1–13.

[12] V. Limkhuansuwan, P. Chaiprasert, Decolorization of molasses melanoidins and palm oil mill effluent phenolic compounds by fermentative lactic acid bacteria, Int. J. Environ. Sci., 22 (2010) 1209–1217.

[13] Y. Zhou, L. Tang, G. Zeng, J. Chen, Y. Cai, G. Zhang. Y. Yang, Y. Liu, C. Zhang, W. Tang, Mesoporous carbon nitride-based biosensor for highly sensitive and selective analysis of phenol and catechol in compost bioremediation, Biosens. Bioelectron., 61 (2014) 519–525.

[14] U.G. Akpan, B.H. Hameed, Parameters affecting the photocatalytic degradation of dyes using TiO_2-based photocatalysts: a review, J. Hazard. Mater., 170 (2010) 520–529.

[15] J. Wang, C. Li, X. Luan, J. Li, B. Wang, L. Zhang, R. Xu, X. Zhang, Investigation on solar photocatalytic activity of TiO_2 loaded composite: TiO_2/Skeleton, TiO_2/Dens, and TiO_2/HAP, J. Mol. Catal. A: Chem., 320 (2010) 62–67.

[16] S. Guan, L. Hao, Y. Lu, H. Yoshida, F. Pan, H. Asanuma, Fabrication of oxygen-deficient TiO_2 coatings with nanofiber morphology for visible-light photocatalysis, Mater. Sci. Semicond. process., 41 (2016) 358–363.

[17] S. Adishkumar, S. Kanmani, J. Rajesh Banu, Solar photocatalytic treatment of phenolic wastewaters: influence of chlorides, sulphates, aeration, liquid volume, and solar light intensity, Desal. Wat. Treat., 52 (2014) 7957–7963.

[18] M.H. Alhaji, K. Sanaullah, S.F. Lim, A. Khan, C.N. Hipolito, M.O. Abdullah, S.A. Bhawani, T. Jamil, Photocatalytic treatment technology for palm oil mill effluent (POME)-a review, Process. Saf. Environ., 102 (2016) 673–686.

[19] C.K. Cheng, M.R. Deraman, K.H. Ng, M.R. Khan, Preparation of titania doped argentum photocatalyst and its photoactivity towards palm oil mill effluent degradation, J. Cleaner Prod., 112 (2016) 1128–1135.

[20] K.H. Ng, M.R. Khan, Y.H. Ng, S.S. Hossain, C.K. Cheng, Restoration of liquid effluent from oil palm agroindustry in Malaysia using UV/TiO_2 and UV/ZnO Photocatalytic systems: a comparative study, J. Environ. Manage., 196 (2017) 674–680.

[21] M.O. Saeed, K. Azizli, M.H. Isa, M.J.K. Bashir, Application of CCD in RSM to obtain optimize treatment of POME using Fenton oxidation process, J. Water Process Eng., 8 (2015) 7–16.

[22] M.O. Saeed, K.A.M. Azizli, M.H. Isa, E.H. Ezechi, Treatment of POME using Fenton oxidation process: removal efficiency, optimization, and acidity condition, Desal. Wat. Treat., 57 (2016) 23750–23759.

[23] S. Mohajeri, H.A. Aziz, M.H. Isa, M.A. Zahed, M.J.K. Bashir, M.N. Adlan, Application of the central composite design for condition optimization for semi-aerobic landfill leachate treatment using electrochemical oxidation, Water Sci. Technol., 61 (2010) 1257–1266.

[24] A. Asadi, A.A.L. Zinatizadeh, M. Hasnain Isa, Performance of intermittently aerated up-flow sludge bed reactor and sequencing batch reactor treating industrial estate wastewater: a comparative study, Bioresour. Technol., 123 (2012) 495–506.

[25] A. Yaqub, M.H. Isa, H. Ajab, Electrochemical degradation of polycyclic aromatic hydrocarbons in synthetic solution and produced water using a Ti/SnO_2-Sb_2O_5-RuO_2 anode, J. Environ. Chem. Eng., 141 (2015) 1–8.

[26] L.P. Wong, M.H. Isa, M.J.K. Bashir, Disintegration of palm oil mill effluent organic solids by ultrasonication: optimization by response surface methodology, Process Saf. Environ. Prot., 114 (2018) 123–132.

[27] M. Yeber, E. Paul, C. Soto, Chemical and biological treatments to clean oily wastewater: optimization of the photocatalytic process using experimental design, Desal. Wat. Treat., 47 (2012) 295–299.

[28] F.E. Ergul, S. Sargın, G. Ongen, F.V. Sukan, Dephenolization and decolorization of olive mill wastewater through sequential batch and co-culture applications, World J. Microbiol. Biotechnol., 27 (2011) 107–114.

[29] F. Venditti, F. Cuomo, A. Ceglie, P. Avino, M.V. Russo, F. Lopez, Visible light caffeic acid degradation by carbon-doped titanium dioxide, Langmuir, 31 (2015) 3627–3634.

[30] W. Li, T. Zeng, Preparation of TiO_2 anatase nanocrystals by $TiCl_4$ hydrolysis with additive H_2SO_4, PLoS ONE, 6 (2011) 1–6.

[31] R. Kamaludin, M.H.D. Othman, S.H.S.A. Kadir, A.F. Ismail, M.A. Rahman, J. Jaafar, Visible-light-driven photocatalytic N-doped TiO_2 for degradation of bisphenol A (BPA) and reactive Black 5 (RB5) dye, Water Air Soil Pollut., 229 (2018) 1–11.

[32] A. Kudo, Y. Miseki, Heterogeneous photocatalyst materials for water splitting, Chem. Soc. Rev., 38 (2009) 253–278.

[33] X. Chen, L. Liu, F. Huang, Black titanium dioxide (TiO_2) nanomaterials, Chem. Soc. Rev., 44 (2015) 1861–1885.

[34] L. Gonzalez-Reyes, I. Hernandez-Perez, L.D. Arceo, H. Dorantes-Rosales, E. Arce-Estrada, R. Suarez-Parra, J.J. Cruz-Rivera, Temperature effects during Ostwald ripening on structural and bandgap properties of TiO_2 nanoparticles prepared by sonochemical synthesis, Mater. Sci. Eng., 175 (2010) 9–13.

[35] L. Li, Y. Chen, S. Jiao, Z. Fang, X. Liu, Y. Xu, G. Pang, S. Feng, Synthesis, microstructure, and properties of black anatase and B phase TiO_2 nanoparticles, Mater. Des., 100 (2016) 235–240.

[36] H. Dong, G. Zeng, L. Tang, C. Fan, C. Zhang, X. He, Y. He, An overview on limitations of TiO_2-based particles for photocatalytic degradation of organic pollutants and the corresponding countermeasures, Water Res., 79 (2015) 128–146.

[37] O. Carp, C.L. Huisman, A. Reller, Photoinduced reactivity of titanium dioxide, Prog. Solid State Chem., 32 (2004) 33–177.

[38] T. Trung, W.J. Cho, C.S. Ha, Preparation of TiO_2 nanoparticles in glycerol-containing solutions, Mater. Lett., 57 (2003) 2746–2750.

[39] K. Sing, Reporting physisorption data for gas/solid systems with special reference to the determination of surface area and porosity (Provisional), Pure Appl. Chem., 54 (1982) 2201–2218.
[40] X.L. Garcia-Montelongo, A. Martinez-de la Cruz, D. Contreras, H.D. Mansilla, Optimized photocatalytic degradation of caffeic acid by sol-gel TiO_2, Water Sci. Technol., 71 (2015) 878–884.
[41] A. Tolosana-Moranchel, J. Anderson, J. Casas, M. Faraldos, A. Bahamonde, Defining the role of substituents on adsorption and photocatalytic degradation of phenolic compounds, J. Environ. Chem. Eng., 5 (2017) 4612–4620.
[42] M.A. Zahed, H.A. Aziz, M.H. Isa, L. Mohajeri, Response surface analysis to improve dispersed crude oil biodegradation, CLEAN-Soil Air Water, 40 (2012) 262–267.
[43] I.A. Appavoo, J. Hu, Y. Huang, S.F.Y. Li, S.L. Ong, Response surface modeling of carbamazepine (CBZ) removal by graphene-P25 nanocomposites/UVA process using central composite design, Water Res., 57 (2014) 270–279.
[44] M.H. Isa, E.H. Ezechi, Z. Ahmed, S.F. Magram, S.R.M. Kutty, Boron removal by electrocoagulation and recovery, Water Res., 51 (2014) 113–123.
[45] J. Wu, H. Zhang, N. Oturan, Y. Wang, L. Chen, M.A. Oturan, Application of response surface methodology to the removal of the antibiotic tetracycline by electrochemical process using carbon-felt cathode and DSA (Ti/RuO_2–IrO_2) anode, Chemosphere, 87 (2012) 614–620.
[46] N. Quici, M.I. Litter, Heterogeneous photocatalytic degradation of gallic acid under different experimental conditions, Photochem. Photobiol. Sci., 8 (2009) 975–984.
[47] V. Nogueira, I. Lopes, T. Rocha-Santos, F. Gonçalves, A. Duarte, R. Pereira, Photocatalytic treatment of olive oil mill wastewater using TiO_2 and Fe_2O_3 nanomaterials, Water Air Soil Pollut., 227 (2016) 88.
[48] S. Ahmed, M. Rasul, W.N. Martens, R. Brown, M. Hashib, Advances in heterogeneous photocatalytic degradation of phenols and dyes in wastewater: a review, Water Air Soil Pollut., 215 (2011) 3–29.
[49] Z. Zheng, B. Huang, J. Lu, Z. Wang, X. Qin, X. Zhang, Y. Dai, M.H. Whangbo, Hydrogenated titania: synergy of surface modification and morphology improvement for enhanced photocatalytic activity, Chem. Commun., 48 (2012) 5733–5735.
[50] H. Cui, W. Zhao, C. Yang, H. Yin, T. Lin, Y. Shan, Y. Xie, H. Gu, F. Huang, Black TiO_2 nanotube arrays for high-efficiency photoelectrochemical water-splitting, J. Mater. Chem. A, 2 (2014) 8612–8616.
[51] M.N. Chong, B. Jin, C.W. Chow, C. Saint, Recent developments in photocatalytic water treatment technology: a review, Water Res., 44 (2010) 2997–3027.
[52] U.I. Gaya, A.H. Abdullah, Heterogeneous photocatalytic degradation of organic contaminants over titanium dioxide: a review of fundamentals, progress, and problems, J. Photochem. Photobiol., C, 9 (2008) 1–12.